Atmos. Chem. Phys. Discuss., https://doi.org/10.5194/acp-2018-1056
Manuscript under review for journal Atmos. Chem. Phys.
Discussion started: 17 December 2018


Atmospheric Chemistry and Physics Discussions

# High time-resolved measurement of stable carbon isotope composition in water-soluble organic aerosols: method optimization and a case study during winter haze in East China

Wenqi Zhang[1,2,3], Yan-Lin Zhang[1,2,3]*, Fang Cao[1,2,3], Yankun Xiang[1,2,3], Yuanyuan Zhang[1,2,3], Mengying Bao[1,2,3], Xiaoyan Liu[1,2,3], Yu-Chi Lin[1,2,3]

1Yale–NUIST Center on Atmospheric Environment, International Joint Laboratory on Climate and Environment Change (ILCEC), Nanjing University of Information Science and Technology, Nanjing 210044, China

2Key Laboratory of Meteorological Disaster, Ministry of Education (KLME)/ Collaborative Innovation Center on Forecast and Evaluation of Meteorological Disasters (CIC-FEMD), Nanjing University of Information Science and Technology, Nanjing 210044, China

3Jiangsu Provincial Key Laboratory of Agricultural Meteorology, College of Applied Meteorology, Nanjing University of Information Science and Technology, Nanjing 210044, China

**Abstract:** Water soluble organic carbon (WSOC) is a significant fraction of organic carbon (OC) in atmospheric aerosols. WSOC is of great interest due to its significant effects on atmospheric chemistry, the Earth's climate and human health. Stable carbon isotope ($\delta^{13}C$) can be used to track the potential sources and investigate atmospheric processes of organic aerosols. In this study, a method of simultaneously measuring the mass concentration and $\delta^{13}C$ values of WSOC from aerosol samples is established by coupling the Gas Bench II preparation device with isotopic ratio mass spectrometry. The precision and accuracy of isotope determination is better than 0.17 ‰ and 0.5 ‰, respectively, for samples containing carbon larger than 5 μg. This method is then applied for the high time-resolution aerosol samples during a severe wintertime haze period in Nanjing, East China. WSOC varies between 3-32 μg $m^{-3}$, whereas $\delta^{13}C_{\text{-WSOC}}$ ranges from -26.24 ‰ to -23.35 ‰. Three different episodes (e.g., namely the Episode 1, the Episode 2, the Episode 3) are identified in the sampling period, showing a different tendency of $\delta^{13}C_{\text{-WSOC}}$ with the accumulation process of WSOC aerosols. The increases in both the WSOC mass concentrations and the $\delta^{13}C_{\text{-WSOC}}$ values in

Atmos. Chem. Phys. Discuss., https://doi.org/10.5194/acp-2018-1056
Manuscript under review for journal Atmos. Chem. Phys.
Discussion started: 17 December 2018


Atmospheric Chemistry and Physics Discussions

the Episode 1 indicate that WSOC is subject to a substantial photochemical aging during the air mass transport. In the Episode 2, the decline of the $\delta^{13}C_{\text{-WSOC}}$ is accompanied by the increase in the WSOC mass concentrations, which is associated with regional-transported biomass burning emissions. In the Episode 3, heavier isotope ($^{13}C$) is exclusively enriched in total carbon (TC) compares to WSOC aerosols. This suggests that water-insoluble carbon may contain $^{13}C$-enriched components such as dust carbonate which is supported by the enhanced $Ca^{2+}$ concentrations and air mass trajectories analysis. The present study provides a novel method to determine stable carbon isotope composition of WSOC and it offers a great potential to better understand the source emission, the atmospheric aging and the secondary production of water soluble organic aerosols.

**Key words:** WSOC, stable carbon, $\delta^{13}C$, aging

## 1. Introduction

Water soluble organic carbon (WSOC) contributes a large fraction (9-75 %) to the organic carbon (OC) (Anderson, et al., 2008; Decesari et al., 2007; Sullivan et al., 2004) and substantially affects the global climate change and human health (Myhre, 2009; Ramanathan et al., 2001). Due to its hydrophilic nature, WSOC has a great impact on the hygroscopic properties of aerosols and promotes to increase the cloud condensation nuclei (CCN) activity (Asa-Awuku et al., 2011). WSOC is a contributor to cardiovascular and respiratory problems because it is easy to be incorporated in biological systems such as human blood and lungs (Mills et al., 2009). Besides, the transport of WSOC is rapid along the surface layer and then impacts the carbon biogeochemical cycling (Wozniak et al., 2008).

Stable carbon isotopic composition ($\delta^{13}C$) is a useful tool to track both potential sources and atmospheric processes of carbonaceous aerosols (Rudolph, 2007; Pavuluri and Kawamura, 2012; Kirillova et al., 2013; Kirillova et al., 2014). WSOC can be emitted as primary organic carbon (POC) and secondary organic carbon (SOC) produced from atmospheric oxidation of volatile organic compounds (VOCs). POC and VOCs may stem from various sources including coal combustion, vehicle emissions, biogenic emissions, marine emissions and biomass burning (Kirillova et al., 2010). Carbonaceous aerosols from coal combustion have an isotope signature from -24.9 ‰ to -



21 ‰ (Cao et al., 2011). Particulate matter emitted from motor vehicles exhibits with isotopes from -26 ‰ to -28 ‰ (Widory, 2006), respectively. Due to the different pathways of metabolism, C3 and C4 plants are distinctly different with $\delta^{13}C$ (on average of -27 ‰ and -13 ‰, respectively [Martinelli et al., 2002; Sousa Moura et al., 2008]). Laboratory studies demonstrate that there is no significant isotope fractionation compared to the plant material during the biomass burning of either C3 plants or C4 plants. Marine organic aerosol sources are enriched with $^{13}C$ (-22 ‰ < $\delta^{13}C$ < -18 ‰, [Miyazaki et al., 2011]) and play an important role in cost sites. In contrast, carbonate carbon is exhibits with pretty high isotopic ratio of -0.3 ‰ (Kawamura et al., 2004), and generally shows a large proportion in dust aerosols. Isotope signatures of particulate matter emitted from these sources may have different effect on the characteristics of $\delta^{13}C$ in ambient WSOC.

In addition, atmospheric processes like photochemical aging and secondary formation may change the constitution and properties of WSOC, as well as the stable carbon isotope of WSOC ($\delta^{13}C_{\text{-WSOC}}$). For instance, the oxidation of primary particles during atmospheric transport (i.e., aging) may make the reacted aerosol more water soluble (De gouw et al., 2008). According to the kinetic isotope effect (KIE), lighter isotopes ($^{12}C$) have the priority to be oxidized and produce isotope depleted particulate matters (Atkinson R., 1986; Kirillova et al., 2013; Fisseha et al., 2009). In that case, secondary formed WSOC would result in lower $\delta^{13}C$ value compared with its precursor. Whereas positive isotopic fractionation may occurs in the atmospheric aging processes during the long range transport. And these are supported by the field measurements and laboratory studies (Pavuluri and Kawamura, 2012). For instance, Rudolph et al. (2003) finds a substantial enrichment of $^{13}C$ in isoprene, a precursor of oxalic acid, after a long range transport compared to that of fresh emitted isoprene. However, the proportion of various sources and atmospheric processes of either primary or secondary WSOC are poorly understood.

Several studies have reported the temporal and spatial variation, complex chemical species, light absorption and thermal characteristics of WSOC, as well as its relationship with other compounds in fine particles (Wozniak et al., 2008; Wang et al., 2006; Zhang et al., 2018; Martinez et al., 2016). However, only few studies focus on the analysis of $\delta^{13}C_{\text{-WSOC}}$ (Kirillova et al., 2014). This is partially due to the limited techniques to analyze the low abundance of WSOC aerosols.



Previous method usually requires large amount of WSOC (e.g., 100 μg) and complicated sample preparation. This detection limit is too high for samples collected in short time period (i.e. high time resolution aerosol samples) or aerosols from remote areas. However, the analysis of the samples containing small carbon content is in urgently need. For example, the $\delta^{13}C_{\text{-WSOC}}$ values of high time resolution samples help to better understand the behavior of WSOC evolution in shorter time scales. Besides, the complicated preparation may bring much more uncertainties to the results of the isotope measurement.

The objectives of this study are: 1) to provide a sensitive, accurate and precise method to measure the WSOC and $\delta^{13}C_{\text{-WSOC}}$ in ambient aerosol samples. 2) to apply this method for analyzing the high time resolution aerosol samples during a severe haze, and therefore to discuss the potential sources and atmospheric processes of WSOC. In addition, the concentrations of inorganic ions and air mass back trajectories coupled with MODIS fire maps are also analyzed to substantiate the results obtained from $\delta^{13}C$ analysis.

## 2. Methods

### 2.1 Standards

Four working standards are used in this study: potassium hydrogen phthalate (KHP), benzoic acid (BA), sucrose ($CH_6$) and sodium oxalate ($C_2$). KHP and BA are widely used as standards of WSOC measurements. Sucrose and oxalic are taken as standards to represent the characteristics of components in atmospheric WSOC (Fowler et al., 2018; Liang et al., 2015; Pathak et al., 2011; Pavuluri and Kawamura, 2012). The carbon isotope composition of these four standards vary from -12.20 ‰ to -30.04 ‰, this is able to cover the majority of the $\delta^{13}C_{\text{-WSOC}}$ values in ambient aerosol samples. Standards are resolved in Milli-Q water (18.2 MΩ quality) to make standard solutions containing 1–100 μg C for testing the method .

### 2.2 Sample preparation for measurement of WSOC mass concentration and $\delta^{13}C_{\text{-WSOC}}$

The overview of the optimized method for measuring WSOC and $\delta^{13}C_{\text{-WSOC}}$ in aerosols are shown in Fig. 1. WSOC on a 20 mm diameter disc is extracted with 6 mL mili-Q water through water-bath ultrasonic for 30 minutes. The extraction is filtered with a 0.22 μm syringe filter to remove particles. 2.0 g potassium persulfate ($K_2S_2O_8$, Aladdin Industrial Corporation, Shanghai)



and 100 μL phosphoric acid (85 % $H_3PO_4$, AR, ANPEL Laboratory Technologies Inc., Shanghai) are dissolved in 50 mL Milli-Q water to make oxidizing solution. The oxidizing solution made within 24 h is added into the filtered extraction to convert organic compounds to $CO_2$, and to remove inorganic carbon resolved in the solution.

To remove $CO_2$ in the solution and the headspace of the sealed sample vial, high-purity helium (Grade 5.0, 99.999 % purity) is flushed into the vial for 5 min. This step is taken within 12 hours after the mixture (oxidizing solution and the sample extraction) to avoid any oxidation under room temperature. High-purity helium is flushed under the water surface and a stainless steel tube is set for the output gas stream. The open end of this tube is submerged in Milli-Q water to prevent any backflow of atmospheric $CO_2$ (Fig. 1., step 5). After flushing, the vials is heated at 100 ˚C for 60 min in the sand bath pot (quartz sand, Y-2, Guoyu, China). The heated vial is stored overnight at room temperature for cooling and condensing the moisture in the headspace before analysis to prevent any damage to the measuring equipment.

### 2.3 Determination of stable carbon isotopic ratios

Gas in the headspace of prepared sample is extracted and purified by Gas Bench II (Gas Bench II, Thermo Fisher Scientific, Bremen, Germany), and introduced into an isotope ratio mass spectrometer (IRMS) (Mat 253, Thermo Fisher Scientific, Bremen, Germany) for $\delta^{13}C_{\text{-}CO2}$ analysis. The extracted gas is purified with a Nafion water trap to remove the water vapor and then loaded into a 100 uL sample loop through an eight-port Valco valve. After 120 s loading time (the duration time from the beginning of the analysis to the first rotation of the eight port in the Gas Bench II.), the eight-port Valco valve rotates every 70 s to inject the sample gas from the loop into a GC column (Poraplot Q fused-silica cap, 25 m, 0.32 mm; Agilent Technologies). The GC column is set at 40 ˚C for $CO_2$ separation from the matrix gases. The separated $CO_2$ is introduced into another Nafion water trap and subsequently enters into the IRMS with an open split. The gas from each vial is detected 10 times in 15 minutes, showing 10 sample peaks after five reference peaks are tested. The isotopic ratios of the first two sample peaks are abandoned considering the possible memory effect of the system. The average value of the last eight peaks is taken as the result of a certain sample determined by GB-IRMS.

### 2.4 Aerosol samples



The aerosol samples are collected during a severe haze in January (from Jan 14$^{th}$ to 28$^{th}$) of 2015 at the suburban of Nanjing, a megacity in East China. The sampling site is located at the Agrometeorological station in the campus of the Nanjing University of Information Science and Technology. It is close to a busy traffic road and surrounded by a large number of industrial factories. $PM_{2.5}$ samples are collected on pre-combusted quartz-fiber filters every 3 hours with a high-volume aerosol sampler (KC100, Qingdao, China) at a flow rate of 1 $m^3$ $min^{-1}$. After sampling, all the filters are wrapped in aluminum foil, sealed in air-tight polyethylene bags and stored at -26 ˚C for later analysis. A field blank is obtained by placing the blank filter in the filter holder for 10 minutes without sampling.

### 2.5 Chemical analysis

$PM_{2.5}$ concentrations are observed at Pukoku Environmental Supervising Station. Concentrations of total carbon (TC) and $\delta^{13}C_{-TC}$ values are analyzed with EA-IRMS (Thermo Fisher Scientific, Bremen, Germany). WSOC mass concentrations are measured with the TOC analyzer (Shimadzu). Ion concentrations are obtained from Ion Chromatograph (IC, Thermo Fisher Scientific, Bremen, Germany). Besides, the meteorological data are observed nearby the sampling site (Enivs automatic meteorological station).

## 3. Method optimization

Wet oxidation method is used to covert the WSOC to $CO_2$ (Sharp J. H., 1973), and the resulting $CO_2$ can be measured by IRMS. This method is adapted from the stable isotope analysis of organic matter in ground water (Lang et al., 2012; Zhou et al., 2015). Several tests are performed to adjust the optimistic conditions for measuring high time-resolved WSOC aerosols with relative low carbon amounts.

### 3.1 Oxidizing agents

In order to quantify the low concentration of WSOC in aerosols, it is critical to reduce the blank effect for minimizing the detection limit of the method. To achieve this goal, some chemical reagents and their blank effects are tested. The blank effect of $H_3PO_4$ is first tested without adding the oxidant in the solution. The carbon content is 0.03-0.04 μgC regardless of the grades (HPLC grade and AR



grade) of $H_3PO_4$. Thus, AR grade with purity of 85 % $H_3PO_4$ is utilized to prepare the oxidizing solution in this method. The amount of carbon in the procedure blank is magnified more than 10 times (0.46-0.63 μgC) after the oxidant agent is added. The average blank is estimated to be 0.5 μgC, suggests that the oxidant contribution to the procedure blank is more than 90%. The blank is much lower than that of methods analyzing isotopes of WSOC in aquatic environment or soil (De Groot, 2004; Polissar et al., 2009; Werner et al., 1999). The smaller carbon content of the blank suggests the possibility to correctly measure the WSOC and $\delta^{13}C_{\text{-WSOC}}$ of samples containing low carbon content.

### 3.2 Flushing methods

To avoid any contamination, the headspace of the sample vial has to be flushed with the high-purity helium to remove the $CO_2$ (both dissolved and gas phase). Two different flushing methods (F1 and F2) are compared here. F1 is a one-step flushing: helium is bubbled under the water surface for 5 min in a sealed vial, and the gas in the headspace is released through a stainless steel tube to the atmosphere. The open end of this tube is submerged in Milli-Q water to balance the air pressure and to prevent any backflow of the atmospheric $CO_2$. F2 requires two steps: the helium is first bubbled under the water surface for 5 min in an open vial to remove dissolved $CO_2$ in the solution. After the vial is sealed, the helium is flushed again into the headspace for 5 min by piercing the septum with a two-hole sample needle. The two holes are performed as the inlet of the helium and the exit of the gas in the headspace, respectively. Since the inlet helium flow is larger than the outflow, the headspace pressure is considered to be greater than 1atm. In that case, the most noticeable difference between F1 and F2 is the air pressure of the headspace.

Different concentrations of KHP are tested to compare the flushing methods. The results of carbon content and isotopic results obtained from F1 and F2 show no significant difference regardless of the concentration of KHP. This represents that F1 and F2 are both able to completely remove the $CO_2$ in the vials. But it has to be noticed that F2 produces excessive air pressure in the headspace, the heating in the following step may increase the risk of gas leak. Gas leaking during the preparation means the loss of carbon content and isotope fractionation, and it has a great effect on both WSOC and $\delta^{13}C$ values. Besides, flushing with F2 takes 5 more minutes for each sample compared to F1. Consequently, F1 is considered as the suitable flushing method to remove $CO_2$



198 dissolved in the solution and the headspace.

199 3.3 Heating time

200 In order to assure complete oxidation of WSOC, duration time for heating the samples is tested
201 with KHP, a widely used WSOC standard which is difficult to oxidize. Figure 2 shows the carbon
202 content and $\delta^{13}C$ values of samples heated from 15 min to 120 min at 100℃. The deformed caps of
203 vials suggest gas leak of overheated samples ( heated for more than 60 min). The gas leak is widely
204 observed in overheated vials, even though the deformation of the caps are not visibly. It is resulted
205 in the high pressure built up in the headspace during the long time of heating. And the gas in the
206 headspace may leak through the flushing holes of the septum. This leaking can be observed from
207 the relatively low carbon content and higher $\delta^{13}C$ values. According to the kinetic isotope effect
208 (KIE), isotope fractionates during the gas leaking. The light carbon isotopes ($^{12}C$) are easier to
209 escape from the vials than the heavy ones ($^{13}C$). $CO_2$ remained in the headspace would be more
210 enriched with heavy isotopes ($^{13}C$) after leaking. On the contrary, heating time less than 60 min is
211 not long enough for the complete oxidation, which is shown in lower carbon content and more
212 variable isotope compositions (Fig. 2.). Therefore, heating for 60 min at 100℃ is found to be most
213 suitable to produce constant results without isotope fractionation.

214 3.4 Waiting time and instrument settings

215 The waiting time of the mixture (aerosol extractions and the oxidizing solution) between step 4
216 and 5 in Fig. 1. is tested to prevent $CO_2$ loss during the flushing. Some of the compounds in aerosol
217 samples could be oxidized at room temperature. The $CO_2$ generated from the mixture before heating
218 could be lost during the flushing step (Sharp, 1973). The ambient sample is tested to detect the room
219 - temperature - oxidized $CO_2$ (Fig. S1.). Replicates of one ambient aerosol sample extraction are
220 mixed with oxidizing agent, and stored at room temperature from 1 to 31 hours before analysis.
221 Samples stored less than 12 h exhibit with carbon content smaller than 0.02 μgC and contributes
222 about 7 % to the amount of procedure blank. When the waiting time is extended to 31 h, up to 2.3
223 μgC is oxidized into $CO_2$ and lost by the flushing in later procedure. The lost carbon content is almost
224 five times of the blank samples and then results in significant isotope fractionation in the final results.
225 Therefore, the mixture should be purged within 12 h to avoid $CO_2$ loss and isotope fractionation.

Atmos. Chem. Phys. Discuss., https://doi.org/10.5194/acp-2018-1056
Manuscript under review for journal Atmos. Chem. Phys.
Discussion started: 17 December 2018


Atmospheric Chemistry and Physics Discussions

Various combinations of different loading time and sample peak numbers are tested through reference gas detection to shorten the analysis in the system. Shorter loading time (30-90 s) and fewer sample peaks (i.e. 5 sample peaks) decrease the sensitivity of mass spectrometry (about 2 μgC lower of carbon content) and the decline of isotopic ratios (~ 0.4 ‰ of $\delta^{13}C$). Thus, 120 s loading time and 10 sample peaks are necessary for precise results, the standard deviation is < 0.03 ‰ for the 10 sample peaks within a run.

### 3.5 Calibration of the results

#### 3.5.1 Blank correction

The blank effects of the WSOC mass concentrations and the $\delta^{13}C_{\text{-WSOC}}$ values are evaluated with peak areas and isotopes. The peak area obtained from the measurement could represent the carbon content in the tested sample/standard. The procedure blank can be corrected according to the mass balance as follows.

$$\delta^{13}C_{meas} \times A_{meas} = \delta^{13}C_{corr} \times (A_{meas} - A_{blk}) + \delta^{13}C_{blk} \times A_{blk} \quad (1)$$

Where $\delta^{13}C_{corr}$, $\delta^{13}C_{meas}$ and $\delta^{13}C_{blk}$ are the blank-corrected $\delta^{13}C$, the measured $\delta^{13}C$ of samples and the $\delta^{13}C$ of procedural blanks, respectively. $A_{meas}$ and $A_{blk}$ denote the peak areas of the samples and blanks, correspondingly.

In order to calibrate the contribution of procedural blanks to the isotope results, $A_{blk}$ and $\delta^{13}C_{blk}$ are calculated with an indirect method (Polissar et al., 2009). KHP ($\delta^{13}C$= -30.04 ‰) and $CH_6$ ($\delta^{13}C$= -12.20 ‰) with various concentrations are measured to calculate $A_{blk}$ and $\delta^{13}C_{blk}$. The wide range of their isotopes can basically cover the $\delta^{13}C_{\text{-WSOC}}$ in most ambient aerosol samples. According to Eq. (1), $\delta^{13}C_{meas}$ can be written as the following:

$$\delta^{13}C_{meas} = \delta^{13}C_{corr} + A_{blk}(\delta^{13}C_{blk} - \delta^{13}C_{corr})/A_{meas} \quad (2)$$

A linear relationship of the $\delta^{13}C$ values and the reciprocal of peak areas ($1/A_M$) is observed from Eq. (2). Based on the keeling plot theory, linear equations of the $\delta^{13}C$ values and the reciprocal of peak areas ($1/A_M$) for the two standards are set up separately. The slopes are represented with $k_1$, $k_2$ and the intercepts are $b_1$, $b_2$.

Atmos. Chem. Phys. Discuss., https://doi.org/10.5194/acp-2018-1056
Manuscript under review for journal Atmos. Chem. Phys.
Discussion started: 17 December 2018


Atmospheric Chemistry and Physics Discussions

$$k_1 = A_{blk} \times (\delta^{13}C_{blk} - \delta^{13}C_{corr-std1})$$
$$k_2 = A_{blk} \times (\delta^{13}C_{blk} - \delta^{13}C_{corr-std2}) \quad (3)$$

$$b_1 = \delta^{13}C_{corr-std1}$$
$$b_2 = \delta^{13}C_{corr-std2} \quad (4)$$

According to Eq. (3) and Eq. (4), $A_b$ and $\delta^{13}C_b$ can be calculated as follows:

$$\delta^{13}C_{blk} = (k_2 \times b_1 - k_1 \times b_2)/(k_2 - k_1) \quad (5)$$

$$A_{blk} = (k_2 - k_1)/(b_1 - b_2) \quad (6)$$

Thus, the blank effects are able to be calibrated with the equation below:

$$\delta^{13}C_{meas} = (\delta^{13}C_{meas} \times A_{meas} - \delta^{13}C_{blk} \times A_{blk})/(A_{meas} \times A_{blk}) \quad (7)$$

3.5.2 Correction of system errors

The $\delta^{13}C$ values of four working standards are measured with both EA and Gas Bench II to correct the system errors. The principle discrepancy of measuring isotopes on different peripherals generally results in system errors. For instance, $\delta^{13}C$ of KHP measured with EA is not comparable with results from Gas Bench II. In this research, more than 10 repetitions of each standard are tested to confirm the $\delta^{13}C$ values on both EA and Gas Bench II. After the blank correction as described in Sec. 3.5.1, the average value of the $\delta^{13}C$ in each group is taken as the final result of the isotopic ratio for the certain standard. The isotope standard curve can be established with the blank corrected results of the four standards (KHP, BA, $CH_6$ and $C_2$). Then the results tested by the two different peripherals can be corrected to the same level of EA. Raw data of the isotopic ratios from Gas Bench II and EA as well as the corrected results are plotted in Fig. 3. Corrected results are closer to EA and the blank effects on small samples are drastically eliminated. After the calibration, the standard deviation of corrected isotopic ratios is lower than 0.17 ‰. The blank effects and the system error are corrected in this way, and the dilution curves of the standards show high precision (0.17 ‰) and low detection limit (5 μgC) of this method.

3.6 QA/QC procedure

A batch of working standards with different carbon contents are measured to evaluate the detection limit, precision, and accuracy of the optimized method in this study (data shown in Fig.



277 3.). The detection limit of WSOC is 5 μgC, which is 10 times of the carbon content of procedural
278 blanks. The average recovery of the working standards is tested to be 97±6 %, suggesting completely
279 oxidation of WSOC without isotope fractionation during the preparation. The precision of the last
280 eight sample peaks in each run is < 0.15 ‰ for standards containing more than 1 μgC. Between runs,
281 the deviation of standards in different carbon contents (> 5 μgC) is < 0.17 ‰. The accuracy is
282 estimated to be better than 0.5 ‰ by comparing the calibrated $\delta^{13}C$ results of Gas Bench II and EA.
283 Isotope results tested by Gas Bench II is slightly smaller compared to the results of EA. As stated
284 above, the procedural blank contains about 0.5 μg WSOC. To conclude, the presented method is
285 considered to be precise and accurate to detect the low abundance of WSOC as well as isotopes in
286 aerosol samples.

287 To test the applicability of this method to the atmospheric WSOC, the ambient aerosol samples
288 collected in Nanjing are analyzed. And the WSOC concentrations are measured with TOC analyzer
289 (Shimadzu) for comparison. Figure 4. shows the scattered plot of WSOC concentrations measured
290 with the two peripherals. The strong correlation ($R^2$=0.95, p<0.01) and the slope (0.86) demonstrate
291 the reliability of measuring WSOC with the presented method. It suggests complete oxidation of
292 WSOC in aerosol samples, which means no significant carbon isotope fractionation happens during
293 the preparation. Moreover, the $\delta^{13}C_{\text{-WSOC}}$ values (between -26.24 ‰ to -23.35 ‰) of ambient
294 aerosols are close to the published data (from -26.5 ‰ to -17.5 ‰) (Kirillova et al., 2013; Kirillova
295 et al., 2014). In that case, the $\delta^{13}C$ values resulted from this method are considered to be effective
296 for ambient WSOC.

297 **4. Sources and atmospheric processes of WSOC**

298 4.1 Temporal variation

299 Time series of $PM_{2.5}$, $\delta^{13}C$ values, chemical tracers and meteorological data observed at the
300 sampling site during the studied period are illustrated in Fig. 5. WSOC ranges from 3.0 to 32.0 μg
301 $m^{-3}$, occupying 49 ±10 % of total carbon in $PM_{2.5}$. The stable carbon isotopes of WSOC and TC vary
302 between -26.24 ‰ to -23.35 ‰ and -26.83 ‰ to -22.25 ‰, respectively. $\delta^{13}C$ values are found to
303 shift over 2 ‰ in 24 hours, 1 ‰ in 3 hours, which is not able to be captured in lower time resolution
304 samples (e.g., 12h or 24h). In that case, this data set can be interpreted with more detailed

Atmos. Chem. Phys. Discuss., https://doi.org/10.5194/acp-2018-1056
Manuscript under review for journal Atmos. Chem. Phys.
Discussion started: 17 December 2018


Atmospheric Chemistry and Physics Discussions

information about the WSOC sources and atmospheric processes. Biomass burning tracer (nss-$K^+$), dust tracer ($Ca^{2+}$), MODIS fire spots and air mass trajectories are analyzed to investigate the potential sources of WSOC. Nss-$K^+$ is used as a proxy of biomass burning (Zhang et al., 2013). Nss-$K^+$ concentrations are evaluated from $Na^+$ contents in the samples according to their respective ratios ($K^+/Na^+$=0.037 *w/w*) in seawater (Osada et. al., 2008).

$$\mathrm{nss-K^+} = [\mathrm{K^+}] - 0.037 \cdot [\mathrm{Na^+}] \quad (8)$$

where $[K^+]$ and $[Na^+]$ are the total measured mass concentrations in collected fine particles. The concentration of nss-$K^+$ is ranged from 0.16 to 6.70 μg $m^{-3}$ with an average of 1.31 μg $m^{-3}$marked in Fig. 5e. The high concentration and intense increase in Jan 24$^{th}$ indicates a significant biomass burning event and will be discussed later.

As shown in Fig. 5., $\delta^{13}C_{\text{-TC}}$ and $\delta^{13}C_{\text{-WSOC}}$ show similar pattern during the sampling period. In general, $\delta^{13}C_{\text{-TC}}$ is slightly lower than $\delta^{13}C_{\text{-WSOC,}}$ and the trend is also observed elsewhere (Fisseha et al., 2009). It is related to the sources and the atmospheric processes during the formation and transformation of carbonaceous particles in the atmosphere. Aerosols emitted from C4 plants biomass burning and marine organic materials are enriched in $^{13}C$. Smith and Epstein (1971) suggest that C4 plants have a mean $\delta^{13}C$ isotope signature of -13 ‰. And carbon emitted from phytoplankton, an example of primary marine aerosol, is exhibited with $\delta^{13}C$ between -22 ‰ to -18 ‰ (Miyazaki et al., 2011). However, January is not a specific time period for C4 plants growing or combustion in East China, indicating small possibility of C4 plants biomass burning as a major source of WSOC aerosols. On the other hand, air parcel transported from marine areas normally have little effect on the aerosol during winter in Nanjing, suggesting the negligible contribution of marine emissions of WSOC (Qin et al., 2016). Therefore, the isotope enriched WSOC sources are not able to explain the high values of $\delta^{13}C_{\text{-WSOC}}$ over $\delta^{13}C_{\text{-TC}}$.

Apart from the sources, the secondary formation (Hecobian et al., 2010; Jimenez et al., 2009; Saarikoski et al., 2008) of WSOC is reported to affect the isotope compositions. Precursors like VOCs can be oxidized with hydroxyl radicals and ozone to produce WSOC in the atmosphere (Pathak et al., 2011). Laboratory and field studies demonstrate that the lighter isotopes have the priority to be oxidized to produce isotope depleted particulates, which also results in the $^{13}C$



enrichment in residual VOCs and $^{13}C$ depleted products (Rudolph et al., 2002). Secondary formation tends to lower the $\delta^{13}C$ of ambient WSOC, thus the secondary formation could not explain the $^{13}C$ enrichment in WSOC compared to TC.

Studies demonstrate that the photochemical aging process during long range transport causes significant enrichment in stable carbon isotope (Aggarwal and Kawamura, 2008; G. Wang et al., 2010). The isotope fractionation is up to 3 ‰ - 7 ‰ of the residual during the photolysis of oxalic acid, a dominant species in WSOC aerosols (Pathak et al., 2011). Due to the hydrophilic property, WSOC is associated with the aerosol aging processes. WSOC/OC ratio is normally considered to represent the aging status (Agarwal et al., 2010; Pathak et al., 2011), it increases with photochemical aging process. The WSOC/OC is 0.67 ±0.12 (Fig. S2.) in this study, which is higher than the aged aerosols with WSOC/OC = 0.41 reported elsewhere (Huang et al., 2012). The high value of WSOC/OC indicates aged aerosols during the sampling period. Thus the photochemical aging process could partially explain the reason of the higher value of $\delta^{13}C_{\text{-WSOC}}$.

According to the principle of mass balance, a $^{13}C$ depleted sources of non-WSOC can also result in the depletion of $^{13}C$ in TC. TC is consist of OC, EC and carbonate carbon (CC) (Huang et al., 2006), and OC can be divided into WSOC and water insoluble OC (WIOC) according to the hydrophilic character (Eq. 9). In most circumstances, CC is negligible to the amount of TC (Huang et al., 2006; Ten Brink et al., 2004), thus non-WSOC component could be presented as Eq. 10.

$$TC = OC + EC + CC = WSOC + WIOC + EC + CC \quad (9)$$

$$TC - WSOC = WIOC + EC \quad (10)$$

WIOC and EC are generally originate from primary emissions (Park et al., 2013; Y. L. Zhang et al., 2014), and their $\delta^{13}C$ values are better representing their sources. In that case, the $^{13}C$ depleted source which only contributes to non-WSOC components is likely to be another reason of $\delta^{13}C_{\text{-TC}}$ depletion during the sampling period.

### 4.2 Three episodes

During the sampling period, three significant haze events (e.g., namely the Episode 1, the Episode 2, the Episode 3) are observed in Nanjing. These 3 episodes show different tendencies of



360 $\delta^{13}C_{\text{-WSOC}}$ variation during the accumulation processes of WSOC aerosols (see Fig. 5.). The Episode
361 1 and 2 are compared here due to the distinct $\delta^{13}C_{\text{-WSOC}}$ trends with WSOC concentrations. In the
362 Episode 3, $^{13}C$ is found to be enriched in TC compared to WSOC ($\delta^{13}C_{\text{-WSOC}} < \delta^{13}C_{\text{-TC}}$, $p<0.01$),
363 which is contrasting to the trend in other periods ($\delta^{13}C_{\text{-WSOC}} > \delta^{13}C_{\text{-TC}}$, $p<0.01$) as explained in Sec.
364 4.1.

365 4.2.1 The Episode 1

366 As for the Episode 1, the $\delta^{13}C_{\text{-WSOC}}$ increases with the mass concentration of WSOC ($r = 0.84$,
367 $p < 0.001$, see Fig. 6d.), indicating the sampling site is impacted by WSOC sources with enriched
368 $^{13}C$ and/or photochemical aged aerosols. As shown in Fig. 6a., air mass trajectories of WSOC with
369 higher $\delta^{13}C_{\text{-WSOC}}$ (>24‰) is originated mainly from northern China, and the northerly wind prevails
370 over this site (Fig. 5g.). During the long-range transport, the studied WSOC mass concentration
371 increases with the $^{13}C$ enrichment of WSOC due to the isotope fractionation in the photochemical
372 aging process. This is supported by the increasing ratio of WSOC/OC (from 0.73 to 0.91) in the
373 Episode 1 (Fig. S2.).

374 According to the higher isotopes ($\delta^{13}C_{\text{-WSOC}} > -24$ ‰) and the corresponding trajectories (Fig.
375 6a.), C4 plants biomass burning ($\delta^{13}C \sim -12$‰, [Martinelli et al., 2002; Sousa Moura et al., 2008])
376 and coal combustion ($\delta^{13}C \sim -24.9$ ‰ to -21 ‰, [Cao et al., 2011]) are considered to be possible
377 sources of WSOC. Nss-$K^+$ is largely originated from plants combustion (Zhang et al., 2013), and is
378 analyzed as a proxy of biomass burning. However, during this period the nss-$K^+$ level ($0.56 \pm 0.41$
379 μg $m^{-3}$) is not significantly increased and is comparable with the average value (1.3 μg $m^{-3}$, Fig.5e).
380 This is also evident by the MODIS fire spots along with the trajectories from northern China (Fig.
381 6a.). Besides, the main crops growing in northern China are mainly C3 plants such as wheat and
382 rice during the sampling period (Chen et al., 2004). Biomass burning contribution of C3 plants
383 would even lower the $\delta^{13}C$ values of WSOC. In that case, open field biomass burning is not
384 considered as a major source of WSOC at the sampling site during the Episode 1. Furthermore,
385 WSOC mass concentrations and $\delta^{13}C_{\text{-WSOC}}$ decreases synchronously with the change of the wind
386 direction (from north to southeast) right after the Episode 1. The prevail of southeast wind breaks
387 the continuous transport of WSOC from northern China. The relatively lower $\delta^{13}C_{\text{-WSOC}}$ values are
388 then observed, which is rather due to a reginal isotope signal of WSOC without a substantial aging.



Besides, the WSOC/OC declines obviously with the isotope after the Episode 1 (Fig. S2.), indicating less contribution of aged aerosols to the sampling site. Therefore, the elevated $\delta^{13}C_{\text{-WSOC}}$ values with the increased WSOC mass concentrations in the Episode 1 are mainly affected by the aged aerosols transported from northern China.

4.2.2 The Episode 2

The $\delta^{13}C_{\text{-WSOC}}$ values show an opposite trend with WSOC mass concentrations ($r = -0.54$, $p < 0.01$, see Fig. 6e.) in the Episode 2. At the beginning of the Episode 2 (Jan 22$^{nd}$), the sampling site is mainly affected by the air mass from the north of Nanjing when WSOC displays the relatively higher $\delta^{13}C_{\text{-WSOC}}$ values. After Jan 22$^{nd}$, the shift of the wind direction and air mass trajectories are well corresponded with the decline of the $\delta^{13}C_{\text{-WSOC}}$ values (Fig. 6b.). The large amount of fire spots in the potential source regions suggest the significant impact of open field biomass burning. It should be noted that the stable carbon isotope composition of C3 plant combustion is relatively low (i.e., $\delta^{13}C$~ -27‰, [Martinelli et al., 2002; Sousa Moura et al., 2008]). $\delta^{13}C_{\text{-WSOC}}$ decreases when air mass travels throughout the regions with higher hot spots and WSOC mass concentration peaks to the maximum. The concentration of nss-$K^+$ has a positive correlation with WSOC ($r=0.82$, $p<0.001$) and a negative correlation with $\delta^{13}C_{\text{-WSOC}}$ ($r = -0.45$, $p<0.05$) during the Episode 2. And the concentration of nss-$K^+$ increases up to 6.7 μg m$^{-3}$, almost 7 times of the average value, indicating a significant biomass burning contribution. These results suggest that biomass burning emission is a major source of WSOC in this period, which also explain the decreasing trend in $\delta^{13}C_{\text{-WSOC}}$. During this period, the WSOC/OC ratio also decline from 0.88 to 0.53 (Fig. S2.), indicating that the increased WSOC is rather from fresh biomass-burning aerosols without a substantial aging process.

4.2.3 The Episode 3

The $^{13}C$ is exclusively enriched ($p<0.01$) in TC (-23.5 ± 0.43 ‰) compared to WSOC (-25.17 ±1.08 ‰) during the Episode 3 (see Fig. 6f.). This might be related with a $^{13}C$-enriched source and/or the aging process of non-WSOC fraction in TC. Non-WSOC fraction is mainly consist of WIOC, EC and carbonate carbon (CC), which should be more stable than WSOC during aging process. Therefore, the aging process of non-WSOC fraction in TC cannot explain the observed difference between $\delta^{13}C$ values of TC and WSOC. Among these carbonaceous species, carbonate



carbon (CC) exhibits with much higher $\delta^{13}C$ values than those in EC and OC (Kawamura et al., 2004). CC could be a significant fraction of dust aerosols, even though it is a very small part of TC in most cases. To study the dust contribution in the Episode 3, $Ca^{2+}$ is determined as an indicator of dust (Huang et al., 2010; Jankowski et al., 2008). $Ca^{2+}$ and TC show similar patterns ($R^2$=0.84, $p<0.01$), indicating dust origins in this period. The argument is also supported by the 48-h backward trajectory analysis(Fig. 6c.). It shows that the air mass mainly originates from a semi-arid region, Mongolia. The photochemical aging of dust aerosols during the long-range transport from Mongolia to Nanjing could possibly promotes the $^{13}C$ enrichment. For short, the enrichment of $^{13}C$ in TC over WSOC is due to a dust event transported to the studied site. According to the mass balance, the isotopic ratio of TC affected by CC in the dust aerosols can be expressed as follows:

$$\delta^{13}C_{-TC} = f_{cc} \times \delta^{13}C_{-CC} + (1 - f_{cc}) \times \delta^{13}C_{-NC} \quad (11)$$

where the $\delta^{13}C_{\text{-TC}}$, $\delta^{13}C_{\text{-CC}}$ and $\delta^{13}C_{\text{-NC}}$ are the stable carbon isotope of TC measured in the Episode 3, isotopic ratio of CC in dust aerosols transported to the studied site and isotope composition of non-CC fractions and $f_{cc}$ represents the contribution of CC to TC. The CC contribution during the Episode 3 is roughly estimated based on few assumptions: 1) the increased TC and $\delta^{13}C_{\text{-TC}}$ is only affected by the dust origin, 2) the average value of $\delta^{13}C_{\text{-TC}}$ (-25 ‰) during the studied period is taken as the $\delta^{13}C_{\text{-NC}}$, 3) $\delta^{13}C_{\text{-CC}}$ in dust sources is 0.3 ‰ (Kawamura et al., 2004). With these considerations, CC contribution is estimated to be up to 10% to TC according to the Eq. 11.

## 5. Conclusions

An optimized method for the detection of WSOC mass concentrations and $\delta^{13}C_{\text{-WSOC}}$ values in aerosol samples with Gas Bench II - IRMS is presented. A two-step correction is applied to calibrate the blank effects and system errors. The procedural blank is estimated to be 0.5 μgC. The detection limit is demonstrated to be 5 μgC by the measurement of working standards with gradient carbon contents. The method yields a high recovery (97±6 %) and therefore a negligible isotope fractionation during the preparation. The precision and the accuracy is better than 0.17 ‰ and 0.5 ‰, separately. WSOC concentrations is consistent (R=0.95) with the measurement conducted by the TOC analyzer.

The optimized method is then applied to analyze the $\delta^{13}C_{\text{-WSOC}}$ of the high time resolution



445 aerosol samples collected during a severe winter haze in East China. WSOC ranged from 3.0 μg m$^{-3}$ to 32.0 μg m$^{-3}$, and $\delta^{13}C_{-WSOC}$ varies between -26.24 ‰ to -23.35 ‰. $^{13}C$ is more enriched in WSOC than that of TC in the majority of the sampling period, indicating aged aerosols and/or $^{13}C$ depleted primary sources of non-WSOC component. Three haze events (e.g., namely the Episode 1, the Episode 2, the Episode 3) are identified with different tendencies of $\delta^{13}C_{-WSOC}$ during the accumulation of WSOC aerosols. Similar patterns of the mass concentrations and the $\delta^{13}C_{-WSOC}$ values in the Episode 1 are demonstrated to be affected by the air mass transported from northern China. This enhancement of $\delta^{13}C_{-WSOC}$ indicates the WSOC aerosols from the studied site is subject to a substantial photochemical aging process during the long range transport. The contrasting trend of the mass and $\delta^{13}C_{-WSOC}$ values in the Episode 2 is interpreted as the contribution of regional biomass burning sources. Due to the dust contribution in the Episode 3, the heavier isotope ($^{13}C$) is exclusively enriched in total carbon (TC) compares to WSOC fraction.

457 The optimized method is demonstrated to be accurate and precise to detect the WSOC mass concentration and its isotope compositions ($\delta^{13}C_{-WSOC}$) in aerosols. Our results demonstrate that the high time-resolved measurement of $\delta^{13}C_{-WSOC}$ can be used to distinguish different atmospheric processes such as photochemical aging and aerosol sources (e.g., biomass burning and dust). However, a quantitative understanding of sources and formation processes of WSOC aerosols is still of great challenge. To reduce knowledge gaps, a combination of multiple methodologies such as high time-resolved measurement of radiocarbon ($^{14}C$) and stable carbon isotope composition ($\delta^{13}C$) together with real-time measurement of chemical compositions (e.g., Aerosol Mass Spectrometers, AMS or Thermal Desorption Aerosol Gas Chromatograh-AMS) is needed in future studies.

466 ***Author contributions.*** YZ conceived and designed the study; YZ, FC and WZ designed the experimental strategy; WZ and YX performed the sampling and isotope measurements; YZ and WZ analyzed the experimental data; YZ and WZ proposed the hypotheses; WZ wrote manuscript with YL; all other co-authors contributed to writing.

470

471 ***Competing interests.*** The authors declare that they have no competing interests.

472

473 ***Acknowledgements.*** This study is supported by the National Key Research and Development



Program of China (2017YFC0212704, 2017YFC0210101), the National Natural Science Foundation of China (Grant nos. 91644103, 41761144056, 41603104), Provincial Natural Science Foundation of Jiangsu (BK20170946), Foundation for Young Scientists of Jiangsu Province (BK20150895) and the funding of Jiangsu Innovation and Entrepreneurship Team.

**Reference:**

Agarwal, S., Aggarwal, S. G., Okuzawa, K., and Kawamura, K.: Size distributions of dicarboxylic acids, ketoacids, α-dicarbonyls, sugars, WSOC, OC, EC and inorganic ions in atmospheric particles over Northern Japan: Implication for long-range transport of Siberian biomass burning and East Asian polluted aerosols. Atmospheric Chemistry and Physics, 10(13), 5839–5858. https://doi.org/10.5194/acp-10-5839-2010,2010.

Aggarwal, S. G., and Kawamura, K.: Molecular distributions and stable carbon isotopic compositions of dicarboxylic acids and related compounds in aerosols from Sapporo, Japan: Implications for photochemical aging during long-range atmospheric transport. Journal of Geophysical Research Atmospheres, 113(14), 1–13. https://doi.org/10.1029/2007JD009365, 2008.

Anderson, C., Dibb, J. E., Griffin, R. J., and Bergin, M. H.: Simultaneous measurements of particulate and gas-phase water-soluble organic carbon concentrations at remote and urban-influenced locations. Geophysical Research Letters, 35(13), 2–5. https://doi.org/10.1029/2008GL033966, 2008.

Atkinson, R.: Kinetics and Mechanisms of the Gas-Phase Reactions of the Hydroxyl Radical with Organic Compounds under Atmospheric Conditions. Chemical Reviews 86(1), 69–201. https://doi.org/10.1021/cr00071a004,1986.

Bao, M., Cao, F., Chang, Y., Zhang, Y. L., Gao, Y., Liu, X., Zhang Y. Y., Zhang W. Q., Tang T. R., Xu Z. F., Liu S. D., Lee X. H., Li J., Zhang G.: Characteristics and origins of air pollutants and carbonaceous aerosols during wintertime haze episodes at a rural site in the yangtze river delta, china. Atmospheric Pollution Research, 8(5), 900-911, https://10.1016/j.apr.2017.03.001, 2017

Cai, Z., Jiang, F., Chen, J., Jiang, Z., and Wang, X.: Weather Condition Dominates Regional $PM_{2.5}$ Pollutions in the Eastern Coastal Provinces of China during Winter, Egu General Assembly Conference.969–980. https://doi.org/10.4209/aaqr.2017.04.0140, 2018.

Cao, J.J., Chow, J.C., Tao, J., Lee, S.C., Watson, J.G., Ho, K.F., Wang, G.H., Zhu, C.S. and Han, Y.M.: Stable carbon isotopes in aerosols from Chinese cities: Influence of fossil fuels. Atmospheric Environment, 45(6), 1359–1363. https://doi.org/10.1016/j.atmosenv.2010.10.056, 2011.

Chen, X.P., Zhou J.C., Wang X. R., Blackmer A. M., & Zhang F. Optimal rates of nitrogen fertilization for a winter wheat-corn cropping system in northern china. Commun Soil Sci Plan, 35(3-4), 583-597, http:// 10.1081/CSS-120029734, 2004.



512 De Groot, P. A.: Handbook of stable isotope analytical techniques (Vol. 1). Elsevier, 2004.

513 Gouw, J. A. D., Brock, C. A., Atlas, E. L., Bates, T. S., Fehsenfeld, F. C., & Goldan, P. D., Holloway
514 J. S., Kuster W. C., Lerner B. M., Matthew B. M., Middlebrook A. M., Onasch T. B., Peltier
515 R. E., Quinn P. K., Senff C. J., Stohl A., Sullivan A. P., Trainer M., Warneke C., Weber R. J.,
516 and Williams E. J.: Sources of particulate matter in the northeastern united states in summer:
517 1. direct emissions and secondary formation of organic matter in urban plumes. Journal of
518 Geophysical Research Atmospheres, 113(D8), D08301. https:// doi:10.1029/2007JD009243,
519 2008.

520 Decesari, S., Mircea, M., Cavalli, F., Fuzzi, S., Moretti, F., Tagliavini, E., and Facchini, M. C.:.
521 Source attribution of water-soluble organic aerosol by nuclear magnetic resonance
522 spectroscopy. Environmental Science and Technology, 41(7), 2479–2484. https://doi.org/Doi
523 10.1021/Es0617111, 2007.

524 Fisseha, R., Saurer, M., Jäggi, M., Siegwolf, R.T., Dommen, J., Szidat, S., Samburova, V. and
525 Baltensperger, U.: Determination of primary and secondary sources of organic acids and
526 carbonaceous aerosols using stable carbon isotopes. Atmospheric Environment, 43(2), 431–
527 437. https://doi.org/10.1016/j.atmosenv.2008.08.041, 2009.

528 Fowler, K., Connolly, P. J., Topping, D. O., and O'Meara, S.: Maxwell–Stefan diffusion: a
529 framework for predicting condensed phase diffusion and phase separation in atmospheric
530 aerosol. Atmospheric Chemistry and Physics, 18(3), 1629–1642, 2018.

531 Hecobian, A., Zhang, X., Zheng, M., Frank, N., Edgerton, E. S., and Weber, R. J.: Water-soluble
532 organic aerosol material and the light-absorption characteristics of aqueous extracts measured
533 over the Southeastern United States. Atmospheric Chemistry and Physics, 10(13), 5965–5977.
534 https://doi.org/10.5194/acp-10-5965-2010, 2010.

535 Huang, H., Ho, K.F., Lee, S.C., Tsang, P.K., Ho, S.S.H., Zou, C.W., Zou, S.C., Cao, J.J. and Xu,
536 H.M.: Characteristics of carbonaceous aerosol in $PM_{2.5}$: Pearl Delta River region,
537 China. Atmospheric research, 104, 227-236. https://doi.org/10.1016/j.atmosres.2011.10.016,
538 2012.

539 Huang, K., Zhuang, G., Li, J., Wang, Q., Sun, Y., Lin, Y., and Fu, J. S.: Mixing of Asian dust with
540 pollution aerosol and the transformation of aerosol components during the dust storm over
541 China in spring 2007. Journal of Geophysical Research, 115, D00K13.
542 https://doi.org/10.1029/2009JD013145, 2010.

543 Huang, L., Brook, J.R., Zhang, W., Li, S.M., Graham, L., Ernst, D., Chivulescu, A. and Lu, G.:
544 Stable isotope measurements of carbon fractions (OC/EC) in airborne particulate: A new
545 dimension for source characterization and apportionment. Atmospheric Environment, 40(15),
546 2690–2705. https://doi.org/10.1016/j.atmosenv.2005.11.062, 2006.

547 Irei, S., Takami, A.,Hayashi, M., Sadanaga, Y., Hara, K., Kaneyasu, N., Sato K., Arakaki T.,
548 Hatakeyama S., Bandow H., Hikida T., and Shimono A.:Transboundary secondary organic
549 aerosol in western japan indicated by the $\delta^{13}C$ of water-soluble organic carbon and the m/z 44
550 signal in organic aerosol mass spectra. Environmental Science & Technology, 48(11), 6273-
551 6281, https://doi.org/10.1021/es405362y, 2014.

552 Jankowski, N., Schmidl, C., Marr, I. L., Bauer, H., and Puxbaum, H.: Comparison of methods for
553 the quantification of carbonate carbon in atmospheric PM10 aerosol samples. Atmospheric
554 Environment, 42(34), 8055–8064. https://doi.org/10.1016/j.atmosenv.2008.06.012, 2008.

555 Jimenez, J.L., Canagaratna, M.R., Donahue, N.M., Prevot, A.S.H., Zhang, Q., Kroll, J.H., DeCarlo,
556 P.F., Allan, J.D., Coe, H., Ng, N.L. and Aiken, A.C.: Evolution of Organic Aerosols in the
557 Atmosphere. Science, 326(5959), 1525–1529. https://doi.org/10.1126/science.1180353, 2009.

558 Kawamura, K., Kobayashi, M., Tsubonuma, N., Mochida, M., Watanabe, T., and Lee, M.: Organic
559 and inorganic compositions of marine aerosols from East Asia: Seasonal variations of water-
560 soluble dicarboxylic acids, major ions, total carbon and nitrogen, and stable C and N isotopic
561 composition. Geochemical Society Special Publications, 9(C), 243–265.
562 https://doi.org/10.1016/S1873-9881(04)80019-1, 2004.

563 Kirillova, E.N., Andersson, A., Sheesley, R.J., Kruså, M., Praveen, P.S., Budhavant, K., Safai, P.D.,
564 Rao, P.S.P. and Gustafsson, Ö.: $^{13}C$- And $^{14}C$-based study of sources and atmospheric
565 processing of water-soluble organic carbon (WSOC) in South Asian aerosols. Journal of
566 Geophysical Research Atmospheres, 118(2), 614–626. https://doi.org/10.1002/jgrd.50130,
567 2013.

568 Kirillova, E. N., Andersson, A., Tiwari, S., Kumar Srivastava, A., Singh Bisht, D., and Gustafsson,
569 Ö.: Water-soluble organic carbon aerosols during a full New Delhi winter: Isotope-base source
570 apportionment and optical properties. Journal of Geophysical Research D: Atmospheres, 119,
571 3476–3485. https://doi.org/10.1002/2013JD021272.Received, 2014.

572 Kirillova, E. N., Sheesley, R. J., Andersson, A., and Gustafsson, Ö. : Natural Abundance $^{13}C$ and $^{14}C$
573 Analysis of Water-Soluble Organic Carbon in Atmospheric. Analytical Chemistry, 82(19),
574 7973–7978. https://doi.org/10.1029/2006GL028325, 2010.

575 Kong, S., Li, X., Li, L., Yin, Y., Chen, K., Yuan, L., Zhang, Y., Shan, Y. and Ji, Y.: Variation of
576 polycyclic aromatic hydrocarbons in atmospheric $PM_{2.5}$ during winter haze period around
577 2014 Chinese Spring Festival at Nanjing: Insights of source changes, air mass direction and
578 firework particle injection. Science of the Total Environment, 520, 59–72.
579 https://doi.org/10.1016/j.scitotenv.2015.03.001, 2015.

580 Lang, S. Q., Bernasconi, S. M., and Früh-Green, G. L.: Stable isotope analysis of organic carbon in
581 small (μg C) samples and dissolved organic matter using a GasBench preparation device.
582 Rapid Communications in Mass Spectrometry, 26(1), 9–16. https://doi.org/10.1002/rcm.5287,
583 2012.

584 Liang, L.L., Guenter, E., Duan, F.K., Ma, Y.L., Cheng, Y., Du, Z.Y. and He, K.B.: Composition and
585 Source Apportionments of Saccharides in Atmospheric Particulate Matter in Beijing. Huanjing
586 Kexue/Environmental Science 36, no. 11: 3935–42.
587 https://doi.org/10.13227/j.hjkx.2015.11.001, 2015.

588 Martinelli, L. A., Camargo, P. B., Lara, L. B. L. S., Victoria, R. L., and Artaxo, P.: Stable carbon and
589 nitrogen isotopic composition of bulk aerosol particles in a C4 plant landscape of southeast
590 Brazil. Atmospheric Environment, 36(14), 2427–2432. https://doi.org/10.1016/S1352-
591 2310(01)00454-X, 2002.



592 Martinez, R. E., Williams, B. J., Zhang, Y., Hagan, D., Walker, M., Kreisberg, N. M., Hering S. V.,
593 Hohaus T., Jayne J. T., Worsnop D. R.:. Development of a volatility and polarity separator
594 (VAPS) for volatility- and polarity-resolved organic aerosol measurement. Aerosol Science
595 and Technology, 50(3), 255–271. https://doi.org/10.1080/02786826.2016.1147645, 2016.

596 Mills, N.L., Donaldson, K., Hadoke, P.W., Boon, N.A., MacNee, W., Cassee, F.R., Sandström, T.,
597 Blomberg, A. and Newby, D.E.: Adverse cardiovascular effects of air pollution. Nature
598 Clinical Practice Cardiovascular Medicine, 6(1), 36–44.
599 https://doi.org/10.1038/ncpcardio1399, 2009.

600 Miyazaki, Y., Kawamura, K., Jung, J., Furutani, H., and Uematsu, M.: Latitudinal distributions of
601 organic nitrogen and organic carbon in marine aerosols over the western North Pacific.
602 Atmospheric Chemistry and Physics, 11(7), 3037–3049. https://doi.org/10.5194/acp-11-3037-
603 2011, 2011.

604 Myhre, G.: Consistency between satellite-derived and modeled estimates of the direct aerosol effect.
605 Science, 325(5937), 187–190. DOI: 10.1126/science.1174461, 2009.

606 Osada, K., Kido, M., Nishita, C., Matsunaga, K., Iwasaka, Y., & Nagatani, M., Nakada H.: Temporal
607 variation of water-soluble ions of free tropospheric aerosol particles over central japan. Tellus
608 Series B-chemical & Physical Meteorology, 59(4), 742–754, https://10.1111/j.1600-
609 0889.2007.00296.x, 2007.

610 Park, S. S., Schauer, J. J., and Cho, S. Y.: Sources and their contribution to two water-soluble organic
611 carbon fractions at a roadway site. Atmospheric Environment, 77, 348–357.
612 https://doi.org/10.1016/j.atmosenv.2013.05.032, 2013.

613 Pathak, R. K., Wang, T., Ho, K. F., and Lee, S. C.: Characteristics of summertime PM2.5 organic
614 and elemental carbon in four major Chinese cities: Implications of high acidity for water-
615 soluble organic carbon (WSOC). Atmospheric Environment, 45(2), 318–325.
616 https://doi.org/10.1016/j.atmosenv.2010.10.021, 2011.

617 Pavuluri, C. M., and Kawamura, K.: Evidence for 13-carbon enrichment in oxalic acid via iron
618 catalyzed photolysis in aqueous phase. Geophysical Research Letters, 39(3), 1–6.
619 https://doi.org/10.1029/2011GL050398, 2012.

620 Pavuluri, C. M., Kawamura, K., Swaminathan, T., and Tachibana, E.: Stable carbon isotopic
621 compositions of total carbon, dicarboxylic acids and glyoxylic acid in the tropical Indian
622 aerosols: Implications for sources and photochemical processing of organic aerosols. Journal
623 of Geophysical Research Atmospheres, 116(18), 1–10. https://doi.org/10.1029/2011JD015617,
624 2011.

625 Polissar, P. J., Fulton, J. M., Junium, C. K., Turich, C. C., and Freeman, K. H.: Measurement of 13
626 C and 15 N Isotopic Composition on Nanomolar Quantities of C and N. Analytical Chemistry,
627 81(2), 755–763. https://doi.org/10.3354/meps240085.water, 2009.

628 Qin, X., Zhang, Z. F., Li, Y. W., Shen, Y., & Zhao, S. H... Sources analysis of heavy metal aerosol
629 particles in north suburb of nanjing. Environmental Science. 37(12): 4467-4474,
630 http://10.13227/j.hjkx.201605237,2016.



631 Ramanathan, V., Crutzen, P. J., Kiehl, J. T., and Rosenfeld, D.: Aerosols, climate, and the
632 hydrological cycle. Science, 294(5549), 2119–2124. DOI: 10.1126/science.1064034, 2001.

633 Rudolph, J.: Gas Chromatography-Isotope Ratio Mass Spectrometry. Volatile Organic
634 Compounds in the Atmosphere, 388–466. Blackwell Publishing: Oxford, UK, 2007.

635 Rudolph, J., Czuba, E., Norman, A. L., Huang, L., and Ernst, D.: Stable carbon isotope composition
636 of nonmethane hydrocarbons in emissions from transportation related sources and
637 atmospheric observations in an urban atmosphere. Atmospheric Environment, 36(7), 1173–
638 1181. https://doi.org/10.1016/S1352-2310(01)00537-4, 2002.

639 Rudolph, J., Anderson R. S., Czapiewski K. V., Czuba E., Ernst D., Gillespie T., Huang L., Rigby
640 C., and Thompson A. E.: The stable carbon isotope ratio of biogenic emissions of isoprene and
641 the potential use of stable isotope ratio measurements to study photochemical processing of
642 isoprene in the atmosphere. Journal of Atmospheric Chemistry, 44(1), 39–55,
643 http://10.1023/A:1022116304550, 2003.

644 Saarikoski, S., Timonen, H., Saarnio, K., Aurela, M., Järvi, L., Keronen, P., Kerminen, V.M. and
645 Hillamo, R.: Sources of organic carbon in fine particulate matter in northern European urban
646 air. Atmospheric Chemistry and Physics, 8(20), 6281–6295. https://doi.org/10.5194/acp-8-
647 6281-2008, 2008.

648 Sharp, J. H.: Total organic carbon in seawater - comparison of measurements using persulfate
649 oxidation and high temperature combustion. Marine Chemistry, 1(3), 211–229.
650 https://doi.org/10.1016/0304-4203(73)90005-4, 1973.

651 Smith, B. N., and Epstein, S.: Two Categories of 13C/12C Ratios for Higher Plants. Plant Physiology,
652 47(3), 380–384. https://doi.org/10.1104/pp.47.3.380, 1971.

653 Sousa Moura, J. mauro, Martens, C. S., Moreira, M. Z., Lima, R. L., Sampaio, I. C. G., Mendlovitz,
654 H. P., and Menton, M. C.: Spatial and seasonal variations in the stable carbon isotopic
655 composition of methane in stream sediments of eastern Amazonia. Tellus B: Chemical and
656 Physical Meteorology, 60(1), 21–31. https://doi.org/10.1111/j.1600-0889.2007.00322.x, 2008.

657 Sullivan, A. P., Weber, R. J., Clements, A. L., Turner, J. R., Bae, M. S., and Schauer, J. J.: A method
658 for on-line measurement of water-soluble organic carbon in ambient aerosol particles: Results
659 from an urban site. Geophysical Research Letters, 31(13), 14–17.
660 https://doi.org/10.1029/2004GL019681, 2004.

661 Ten Brink, H., Maenhaut, W., Hitzenberger, R., Gnauk, T., Spindler, G., Even, A., Chi, X., Bauer,
662 H., Puxbaum, H., Putaud, J.P. and Tursic, J: INTERCOMP2000: The comparability of
663 methods in use in Europe for measuring the carbon content of aerosol. Atmospheric
664 Environment, 38(38), 6507–6519. https://doi.org/10.1016/j.atmosenv.2004.08.027, 2004.

665 Wang, G., Xie, M., Hu, S., Gao, S., Tachibana, E., and Kawamura, K.: Dicarboxylic acids, metals
666 and isotopic compositions of C and N in atmospheric aerosols from inland China: Implications
667 for dust and coal burning emission and secondary aerosol formation. Atmospheric Chemistry
668 and Physics, 10(13), 6087–6096. https://doi.org/10.5194/acp-10-6087-2010, 2010.



669 Wang, H., Kawamura, K., and Shooter, D.: Wintertime organic aerosols in Christchurch and
670 Auckland, New Zealand: Contributions of residential wood and coal burning and petroleum
671 utilization. Environmental Science and Technology, 40(17), 5257–5262.
672 https://doi.org/10.1021/es052523i, 2006.

673 Wang, Y., Jia, C., Tao, J., Zhang, L., Liang, X., Ma J., Gao H., Huang T., Zhang K.:Chemical
674 characterization and source apportionment of pm2.5 in a semi-arid and petrochemical-
675 industrialized city, northwest china. Science of The Total Environment, 573, 1031-1040,
676 10.1016/j.scitotenv.2016.08.179,2016.

677 Werner, R. A., Bruch, B. A., and Brand, W. A.: ConFlo III - an interface for high precision $\delta^{13}C$ and
678 $\delta^{15}N$ analysis with an extended dynamic range. Rapid Communications in Mass Spectrometry,
679 13(13), 1237–1241. https://doi.org/10.1002/(SICI)1097-0231(19990715)13:13<1237::AID-
680 RCM633>3.0.CO;2-C, 1999.

681 Widory, D.: Combustibles, fuels and their combustion products: A view through carbon isotopes.
682 Combustion Theory and Modelling, 10(5), 831–841.
683 https://doi.org/10.1080/13647830600720264, 2006.

684 Wozniak, A. S., Bauer, J. E., Sleighter, R. L., Dickhut, R. M., and Hatcher, P. G.: Molecular
685 characterization of aerosol-derived water soluble organic carbon using ultrahigh resolution
686 electrospray ionization Fourier transform ion cyclotron resonance mass spectrometry.
687 Atmospheric Chemistry and Physics, 8(2), 5099–5111. https://doi.org/10.5194/acp-8-5099-
688 2008, 2008.

689 Yu, S., Zhang, Q., Yan, R., Wang, S., Li, P., & Chen, B.,Liu W., Zhang X.: Origin of air pollution
690 during a weekly heavy haze episode in hangzhou, china. Environmental Chemistry Letters,
691 12(4), 543-550, 10.1007/s10311-014-0483-1, 2014.

692 Zeng, Y., & Hopke, P. K.: A study of the sources of acid precipitation in ontario, canada.
693 Atmospheric Environment, 23(7), 1499-1509, 10.1016/0004-6981(89)90409-5,1989.

694 Zhang, F., Cheng, H. R., Wang, Z. W., Lv, X. P., Zhu, Z. M., & Zhang, G., et al.: Fine particles (pm
695 2.5) at a cawnet background site in central china: chemical compositions, seasonal variations
696 and regional pollution events. Atmospheric Environment, 86(3), 193-202,
697 10.1016/j.atmosenv.2013.12.008, 2014.

698 Zhang, R., Jing, J., Tao, J., Hsu, S. C., Wang, G., & Cao, J. J., Lee C. S. L., Zhu L., Chen Z. M.,
699 Zhao Y., Shen Z. X.: Chemical characterization and source apportionment of pm2.5 in Beijing:
700 seasonal perspective. Atmospheric Chemistry and Physics, 13(14), 7053-7074, 10.5194/acp-
701 13-7053-2013, 2013.

702 Zhang, Y.L., El-Haddad, I., Huang, R.J., Ho, K.F., Cao, J.J., Han, Y.M., Zotter, P., Bozzetti, C.,
703 Daellenbach, K.R., Slowik, J.G., Salazar, G., Prévôt, A.S. and Szidat, S.: Large contribution
704 of fossil fuel derived secondary organic carbon to water soluble organic aerosols in winter
705 haze in China. Atmospheric chemistry and physics, 18(6), pp.4005-4017.
706 https://doi.org/10.5194/acp-18-4005-2018, 2018.

707 Zhang, Y.L., Li, J., Zhang, G., Zotter, P., Huang, R.J., Tang, J.H., Wacker, L., Prévôt, A.S. and Szidat,



S.: Radiocarbon-based source apportionment of carbonaceous aerosols at a regional background site on Hainan Island, South China. Environmental Science and Technology, 48(5), 2651–2659. https://doi.org/10.1021/es4050852, 2014.

Zhou, Y., Guo, H., Lu, H., Mao, R., Zheng, H., and Wang, J.: Analytical methods and application of stable isotopes in dissolved organic carbon and inorganic carbon in groundwater. Rapid Communications in Mass Spectrometry, 29(19), 1827–1835. https://doi.org/10.1002/rcm.7280, 2015.

Atmos. Chem. Phys. Discuss., https://doi.org/10.5194/acp-2018-1056
Manuscript under review for journal Atmos. Chem. Phys.
Discussion started: 17 December 2018


Atmospheric Chemistry and Physics Discussions

716 **Table 1.** Various blank preparation with results.

| Identifier | Oxidant [a] | Acid [b] | C content (μgC) |
|---|---|---|---|
| Mili-Q water | - | - | ND* |
| Mili-Q water | - | - | ND* |
| Mili-Q water +Acid-1 | - | 100 uL 85 % $H_3PO_4$, AR | 0.04 |
| Mili-Q water +Acid-1 | - | 100 uL 85 % $H_3PO_4$, AR | 0.04 |
| Mili-Q water +Acid-2 | - | 100 uL 85 % $H_3PO_4$, HPLC | 0.03 |
| Mili-Q water +OX+Acid-1 | 2.0 g $K_2S_2O_8$ | 100 uL 85 % $H_3PO_4$, AR | 0. 63 |
| Mili-Q water +OX+Acid-1 | 2.0 g $K_2S_2O_8$ | 100 uL 85 % $H_3PO_4$, AR | 0.54 |
| Mili-Q water +OX+Acid-1 | 2.0 g $K_2S_2O_8$ | 100 uL 85 % $H_3PO_4$, AR | 0.46 |
| Mili-Q water +OX+Acid-2 | 2.0 g $K_2S_2O_8$ | 100 uL 85 % $H_3PO_4$, HPLC | 0.63 |
| Mili-Q water +OX+Acid-2 | 2.0 g $K_2S_2O_8$ | 100 uL 85 % $H_3PO_4$, HPLC | 0.56 |
| Mili-Q water +OX+Acid-2 | 2.0 g $K_2S_2O_8$ | 100 uL 85 % $H_3PO_4$, HPLC | 0.58 |

717 [a, b] oxidant and acid are added to 50 mL Mili-Q water.

718 ND*：Not detected

719

Atmos. Chem. Phys. Discuss., https://doi.org/10.5194/acp-2018-1056
Manuscript under review for journal Atmos. Chem. Phys.
Discussion started: 17 December 2018


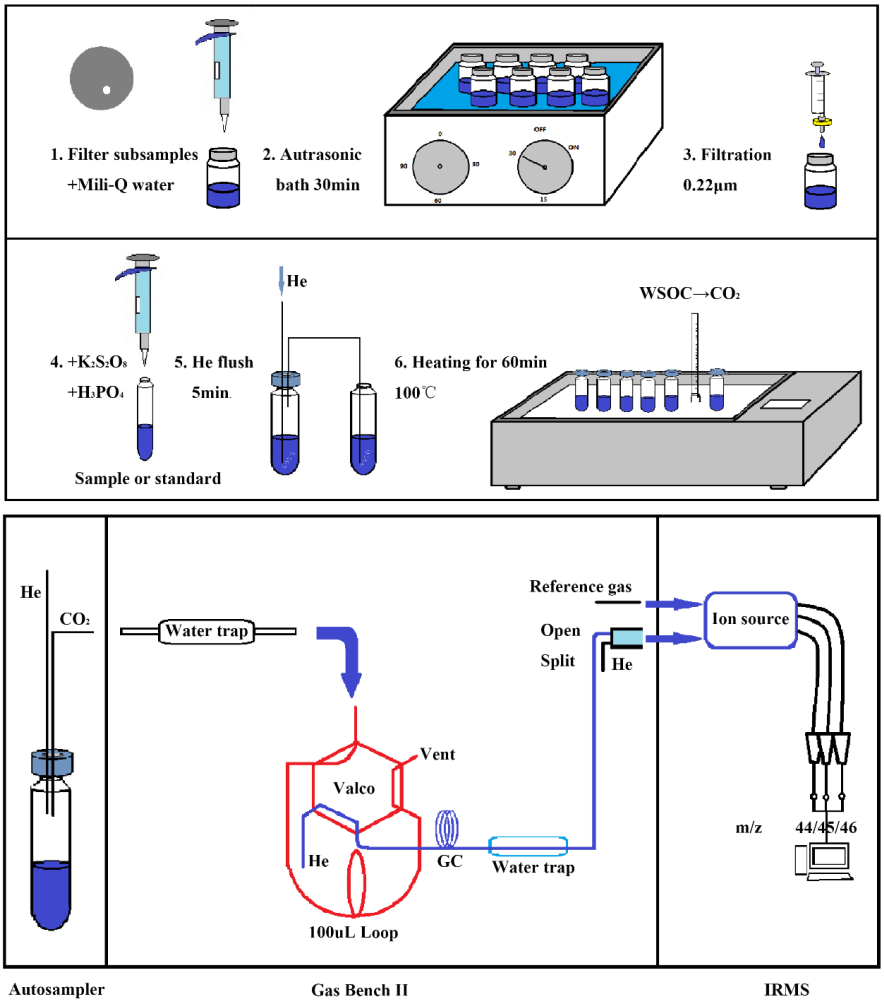


720

721 **Figure 1.** Schematic of the optimized method for the measurement of WSOC mass concentrations

722 and the $\delta^{13}C_{-WSOC}$ values.

723

Atmos. Chem. Phys. Discuss., https://doi.org/10.5194/acp-2018-1056
Manuscript under review for journal Atmos. Chem. Phys.
Discussion started: 17 December 2018


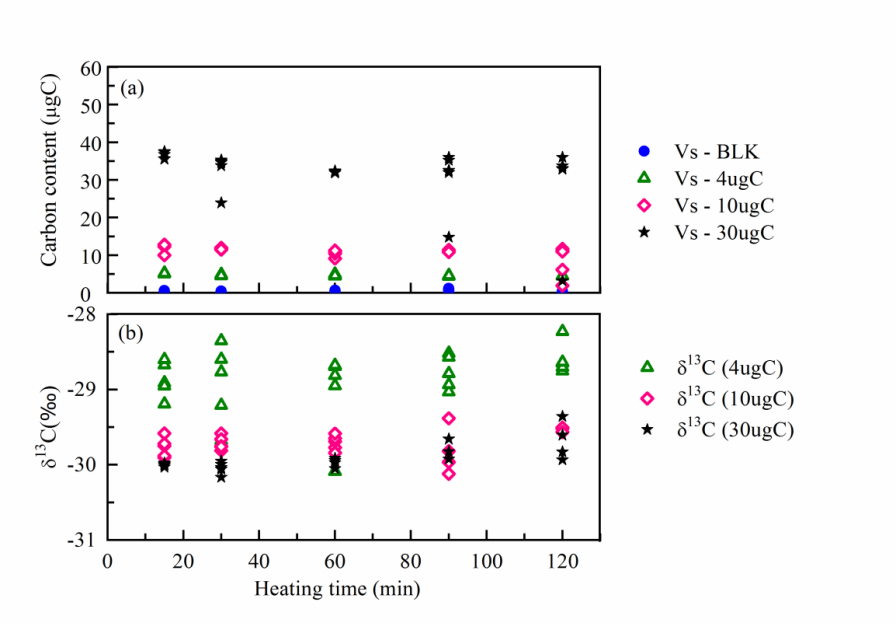


724

725 **Figure 2.** Carbon contents (a) and isotopic ratios (b) of KHP after different heating time.

726

Atmos. Chem. Phys. Discuss., https://doi.org/10.5194/acp-2018-1056
Manuscript under review for journal Atmos. Chem. Phys.
Discussion started: 17 December 2018


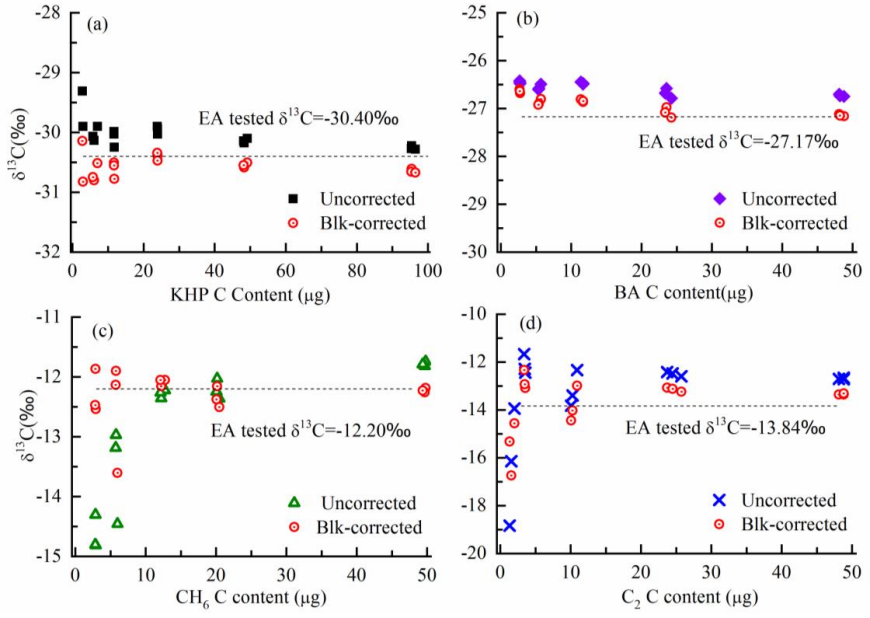


727

728 **Figure 3.** Isotope results before and after the two-step correction of the four standards.

729 (a. KHP, b. BA, c. $CH_6$, d. $C_2$. Red circle with a spot represents the two-step corrected isotopic ratios;

730 ■,◆,△,× represent the raw data from Gas Bench II; the dotted line represents the blank corrected

731 $\delta^{13}C$ values tested by EA)

732

Atmos. Chem. Phys. Discuss., https://doi.org/10.5194/acp-2018-1056
Manuscript under review for journal Atmos. Chem. Phys.
Discussion started: 17 December 2018


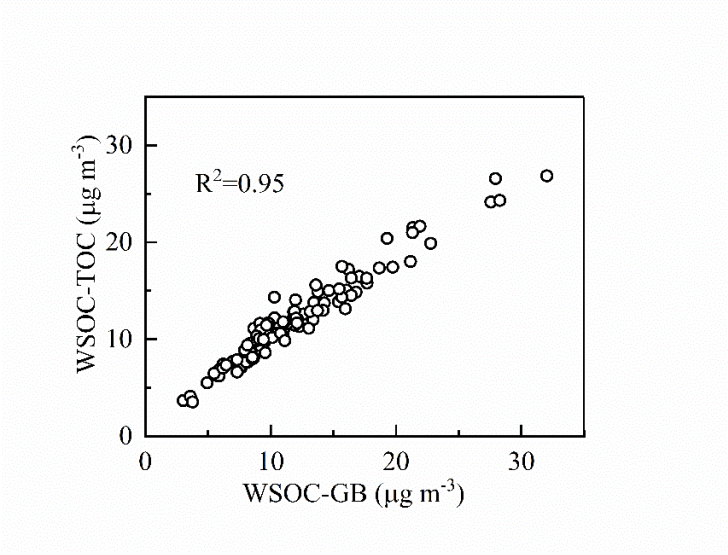


733

734 **Figure 4.** Correlation of WSOC mass concentrations measured with Gas Bench II - IRMS and

735 TOC analyzer.

736

Atmos. Chem. Phys. Discuss., https://doi.org/10.5194/acp-2018-1056
Manuscript under review for journal Atmos. Chem. Phys.
Discussion started: 17 December 2018


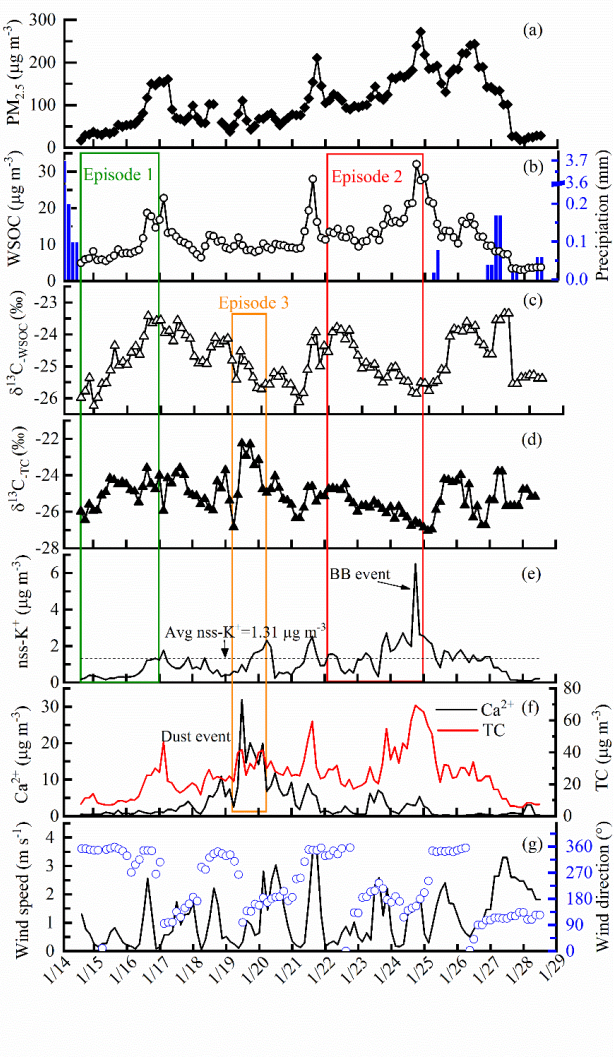


737

738 **Figure 5.** Time series of $PM_{2.5}$, WSOC, precipitation, $\delta^{13}C$ values, nss-$K^+$, $Ca^{2+}$, TC, wind speed
739 and wind direction at the sampling site during the studied period. (The time period framed with the
740 rectangles is defined as the Episode 1 (green), the Episode 2 (red) and the Episode 3 (orange). The
741 dotted line in 5e is the average value of nss-$K^+$ during the studied period. The high concentration
742 and intense increase of nss-$K^+$ in the Episode 2 indicate a significant biomass burning (BB) event,
743 and is marked with "BB event" in 5e. The similar trends of $Ca^{2+}$ and TC suggest a dust event in the
744 Episode 3.**)**

Atmos. Chem. Phys. Discuss., https://doi.org/10.5194/acp-2018-1056
Manuscript under review for journal Atmos. Chem. Phys.
Discussion started: 17 December 2018


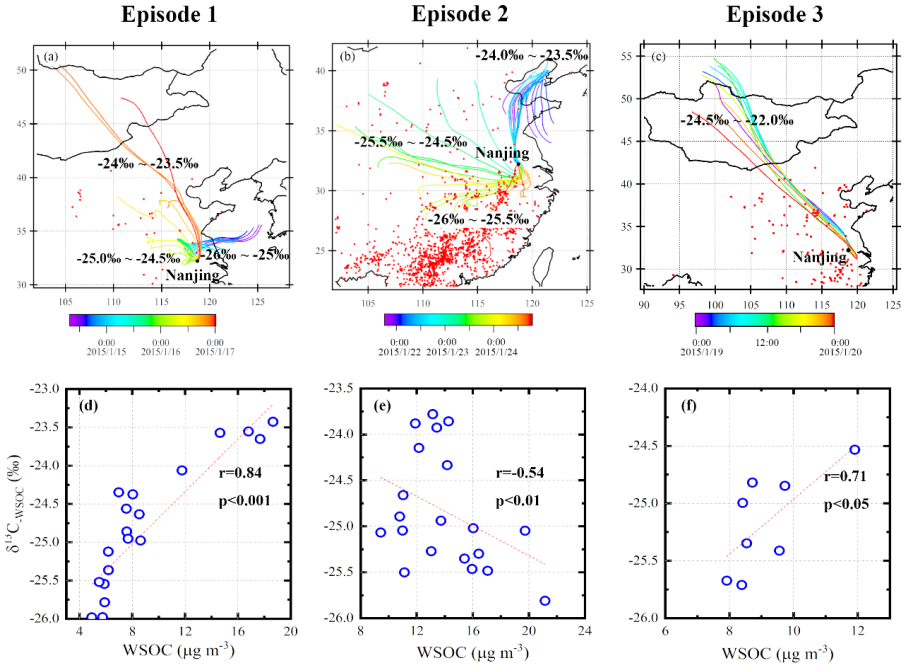


**Figure 6.** 48h-air mass back trajectories at 500m and MODIS fire maps in the three episodes and the corresponding relationship between WSOC and $\delta^{13}C_{\text{-WSOC}}$.

(a, b and c represent the back trajectories and the fire maps of the Episode 1, 2 and 3, separately. The colors of the back trajectories are marked according to the time of the specific trajectory. Red points represent the fire spots in each episode obtained from the Fire Information for Resource Management System (FIRMS) derived from the Moderate Resolution Imaging Spectroradiometer. The range of the $\delta^{13}C$ values obtained from the trajectories are labeled: the marked isotopic ratios are the $\delta^{13}C_{\text{-WSOC}}$ values (for a and b) and the $\delta^{13}C_{\text{-TC}}$ values (for c). d, e and f are the correlation between WSOC and $\delta^{13}C_{\text{-WSOC}}$ in each episode.)